

RESULTS FROM STAR FROM THE FIRST YEAR OF RHIC RUNNING*

LEE BARNBY

for the STAR and STAR-RICH Collaborations

Kent State University, Kent, OH 44242, USA

<http://www.star.bnl.gov>

(Received May 6, 2002)

The STAR detector at RHIC has made a wide variety of measurements from $\sqrt{s_{NN}} = 130$ GeV Au + Au collisions. The overview presented here focuses on hadron production. The yields and spectra of various hadronic species have been measured giving information on the properties and evolution of the fireball created in the collision.

PACS numbers: 25.75.Dw, 25.75.Ld

1. Introduction

Heavy ion collisions at high energy are expected to lead to the formation of a Quark Gluon Plasma (QGP) [1]. The Relativistic Heavy Ion Collider (RHIC) at Brookhaven National Laboratory provided Au + Au collisions at $\sqrt{s_{NN}} = 130$ GeV which should produce sufficiently high energy densities for plasma formation to occur. The Solenoidal Tracker at RHIC (STAR) is a large experiment built to search for signatures of QGP formation. The initial focus is on measuring hadron production in order to understand the properties of the system which is created.

2. The STAR experiment

The STAR experiment has capabilities for detecting a large fraction of the charged particles produced at mid-rapidity. The main tracking detector is a large Time Projection Chamber (TPC) situated in a 0.25 T solenoidal magnetic field as shown in figure 1. The ionization caused by charged tracks

* Presented at the Cracow Epiphany Conference on Quarks and Gluons in Extreme Conditions, Cracow, Poland, January 3-6, 2002.

crossing the TPC is collected in up to 45 samples which enables pions, kaons and protons to be identified at low momentum as shown in figure 2. Pions and protons can be separated up to $1.0 \text{ GeV}/c$ and pions and kaons up to $0.7 \text{ GeV}/c$. A smaller acceptance device at mid-rapidity, the Ring Imaging Cherenkov (RICH), with $\Delta\phi = 20^\circ$ can identify particles at higher momentum by measuring the emitted Cherenkov light. In this case pions and protons may be separated up to $5 \text{ GeV}/c$ and pions and kaons up to $3 \text{ GeV}/c$. Two Zero Degree Calorimeters (ZDCs) are situated 18 m from the center of the TPC along the beam line, in both directions. The ZDCs detect the spectator neutrons from the collision and thus a valid collision requires a signal from both ZDCs. A Central Trigger Barrel (CTB) of scintillator slats surrounds the TPC and provides a fast signal proportional to the multiplicity which allows central collisions to be triggered on. The ZDC *versus* CTB response in figure 3 shows the anti-correlation between these two signals. The signal is monotonic in the CTB response but the ZDC signal is double-valued being minimal for both the most central and most peripheral collisions. In both these cases there are few spectator neutrons. Central collisions were triggered by requiring a high CTB signal in coincidence with a low ZDC response.

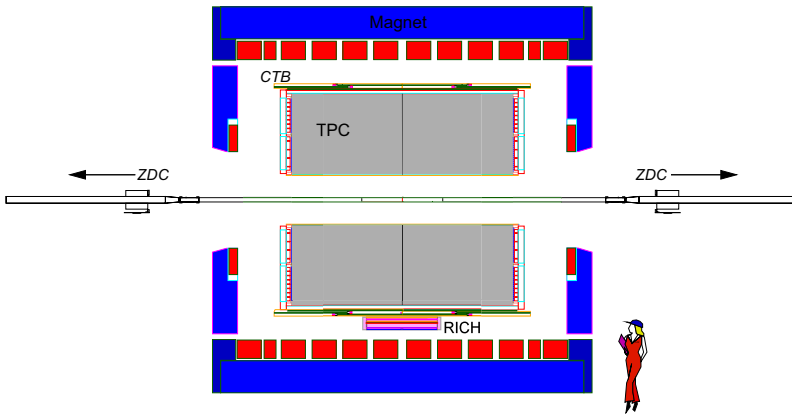


Fig. 1. Cross-sectional view of the STAR detector.

In addition to detecting and identifying single charged particles it is possible to make measurements of weakly decaying strange particles via their decays into charged particles. Each pair of charged tracks is extrapolated back towards the collision vertex in order to find any possible secondary decay vertices at which the kinematic properties of the parent particle can be calculated. This technique, and variations on it, enable the reconstruction of K_S^0 , Λ , Ξ^- , Ω^- and their anti-particles. In all cases where yields are shown the raw yield had to be corrected for the combined detector acceptance and

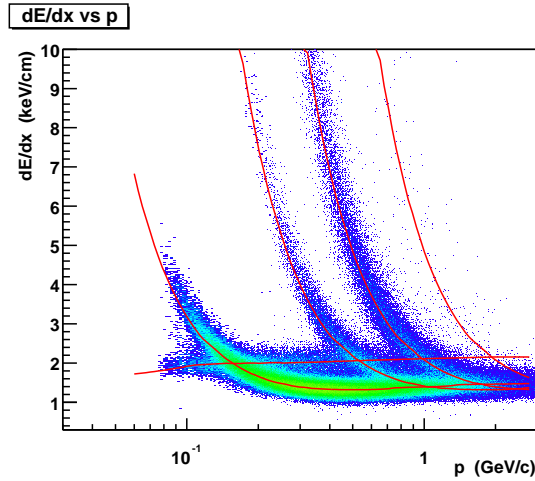


Fig. 2. Energy loss in the TPC as a function of momentum.

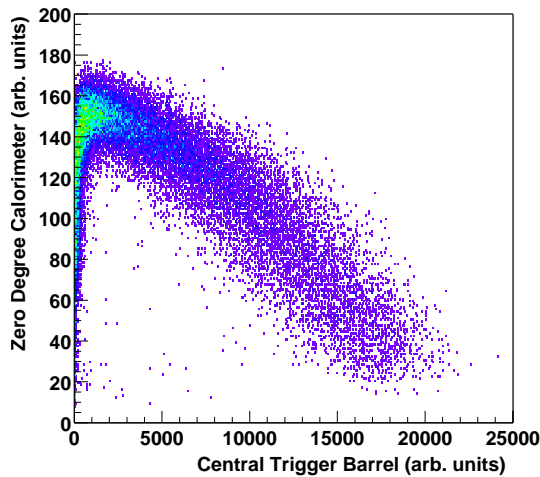


Fig. 3. ZDC response *versus* CTB response.

reconstruction efficiency. This was done by generating particles in accordance with a known distribution and passing them through a full GEANT simulation of the experiment followed by a detailed detector response simulation. The resulting output was then mixed with real raw data on the ADC level and the full reconstruction software run in order to find the fraction of particles reconstructed. For single particles the combined correction was around 70–80% depending on p_T .

3. Baryon number

One of the first interesting topics which can be addressed with the data is to look at the baryon transport or stopping. In the absence of any stopping the anti-baryon/baryon (\bar{B}/B) ratios would be one. In a thermal description of particle production [2] this would correspond to a baryon chemical potential (μ_B) of zero. Positive values of μ_B cause the ratio to be less than one. Preliminary anti-baryon/baryon ratios at mid-rapidity for the 11% most central collisions are shown in figure 4 along with results from SPS collisions at $\sqrt{s_{NN}} = 17$ GeV [3,4]. These results indicate that there is a positive baryon chemical potential presumably due to the transport of baryons from the initial state to mid-rapidity. The mechanism for this is not well understood.

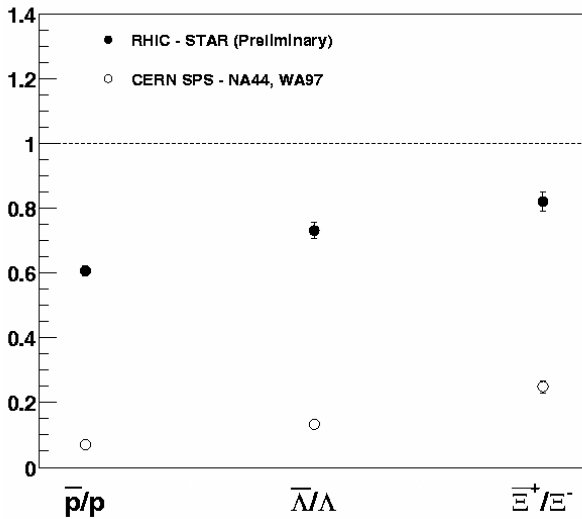


Fig. 4. Anti-baryon/baryon ratios.

Figure 5 shows the \bar{p}/p as a function of p_T for the 14% most central events. The TPC and RICH results together do not indicate any drop in the ratio at higher p_T . Such a drop is predicted [5] due to the presumed different production mechanisms for anti-protons and protons because protons contain valence quarks and the ratio of gluon to quark densities decreases with higher p_T in jets. It will be interesting to extend this measurement to higher p_T and also to look at the $\bar{\Lambda}/\Lambda$ ratio which should also show a similar effect.

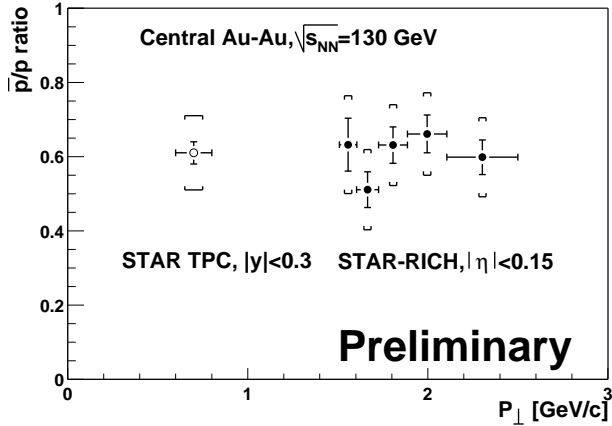


Fig. 5. Anti-proton/proton ratio as a function of p_T .

4. Hadron production

The multiplicity and single particle p_T distributions of hadrons contain information on the characteristics of the fireball. The pseudo-rapidity distribution for negative hadrons from the 5% most central collisions is shown in figure 6 for the measured portion, $p_T > 100$ MeV/c, and the extrapolation to full p_T . The η distribution is almost constant as expected from a boost in-

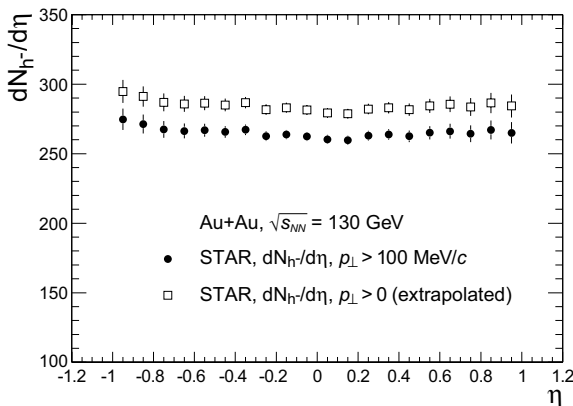


Fig. 6. $dN/d\eta$ for negative hadrons.

variant source. This is in contrast to what was found for Pb+Pb collisions at $\sqrt{s_{NN}} = 17$ GeV where the distributions were found to peak at mid-rapidity. The pion rapidity distribution shown in figure 7 reinforces this interpretation. Establishing this boost invariance is important as it is a simplifying assumption of many models. The h^- pseudo-rapidity density at mid-rapidity

for $p_T > 100$ MeV/c, $dN/d\eta|_{\eta=0}$ of $261 \pm 1(\text{stat.}) \pm 17(\text{sys.})$ [6] is substantially higher than that for both $p + \bar{p}$ (adjusted to the same energy) [7] and Pb+Pb collisions at $\sqrt{s_{NN}} = 17$ GeV [8]. The result is in agreement with the total charged particle yields reported by others [9, 10] once the result from a similar analysis of positively charged particles is added.

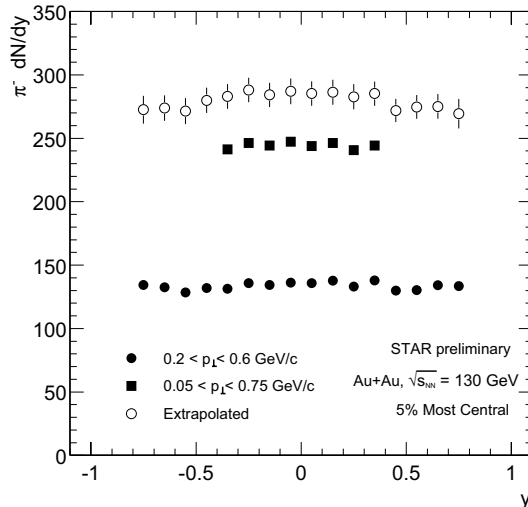


Fig. 7. Pion yields as a function of rapidity.

5. Identified particle spectra

The momentum spectrum of each particle reflects the distribution when elastic interactions ceased, a point in the evolution of the system known as thermal freeze-out. Prior to this there was also the chemical freeze-out point at which inelastic collisions cease and the number of each species is frozen. All the measurements so far indicate that the composition of fireball does not change with the collision centrality and thus the size of the system created. As an example the ratio in the yields of Λ to h^- [11] is constant making it likely that the amount of strangeness produced is also constant. The shape of the spectra on the other hand do show a dependence on system size as was reported for example in [12]. All the spectra appear to exhibit a thermal behaviour and the distributions in transverse mass ($m_T = \sqrt{p_T^2 + m^2}$) can be fitted reasonably well with an exponential over some range in m_T , giving an inverse slope parameter T_{eff} . This can be interpreted as an effective temperature composed of a thermal temperature T_{th} and a radial flow parameter β [13]. The parameters extracted from STAR data are shown in figure 8 along with those from Pb + Pb collisions at

$\sqrt{s_{NN}} = 17$ GeV [14]. The flow interpretation made for the SPS data, where there is a mass dependence to the β term, also seems to be applicable here although the corresponding inverse slopes are systematically higher. This would indicate that the radial flow is stronger in RHIC collisions. This flow picture also explains the change of shape, a flattening of the momentum spectra, with increasing centrality. In both SPS and RHIC data the multi-strange baryons appear to fall below a linear trend which has been interpreted as being due to the a lower re-scattering cross-section for these particles.

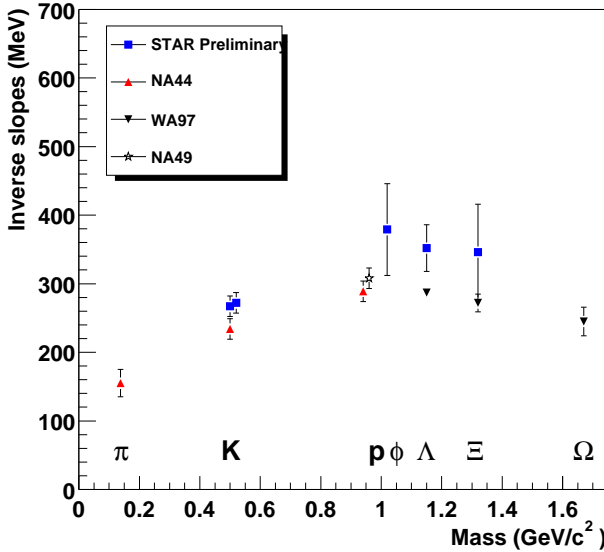


Fig. 8. Inverse slope parameters as a function of particle mass.

There are however some differences to the pattern observed at the SPS. The STAR \bar{p} measurement [12] extracted an inverse slope parameter of 565 MeV, much larger than that at the SPS [14,15]. The reason for this seems to be that the radial flow has become strong enough to not only cause a flattening of the spectra but also to introduce a curvature at low m_T . This causes the extracted slope parameter to become dependent on the range of the fit. In the \bar{p} case this range is only $0.25 < p_T < 0.95$ causing the anomalously large value of T_{eff} compared to the similar mass Λ . There has been some success in modelling these spectra one of which is to use a model inspired by hydrodynamics [16]. In this model the velocity profile is dependent on the radial distance from the centre of fireball with $\beta_r = \beta_s \sqrt{r/R}$ where β_s is the surface velocity at the surface radius, R . Figure 9 shows some m_T spectra with the results of a combined fit to the data. This

model is not unique in reproducing the data, see for example [17]. The integrated yields are well described by thermal models [18] which find a chemical freeze-out temperature of 170 MeV.

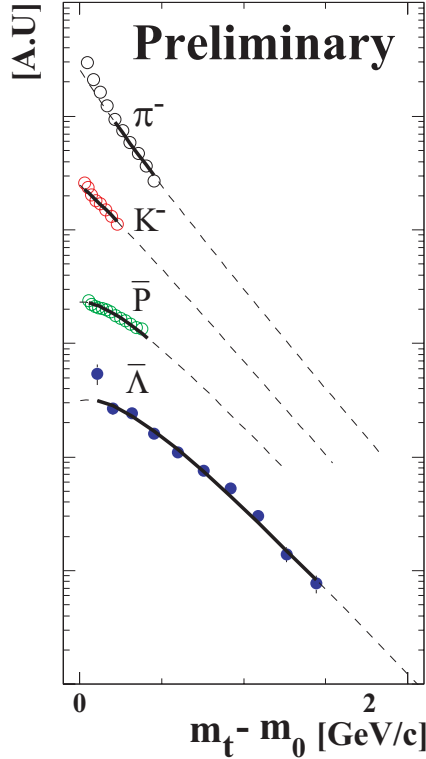


Fig. 9. Measured particle spectra with fits from hydrodynamic model.

6. Elliptic flow

The azimuthal anisotropy in the momentum distribution for non-central collisions is thought to be sensitive to the early evolution of the system. The observable of interest is the second Fourier coefficient, v_2 , known as elliptic flow. The distribution of v_2 as a function of p_T [19] is shown in figure 10. The behaviour of pions and protons is clearly different with the pions showing an almost linear dependence. As expected the kaons lie in between. The fits are from a blast wave model discussed in [19] where it was found that a modification to include a spatially anisotropic freeze-out surface in addition to the azimuthal velocity variation give a better fit to the data. The distribution of v_2 for charged particles up to a p_T of 4.5 GeV/c

is shown in figure 11. Above a p_T of 1.5–2.0 GeV/c the data points depart from the hydrodynamic predictions indicating that such a description is no longer applicable.

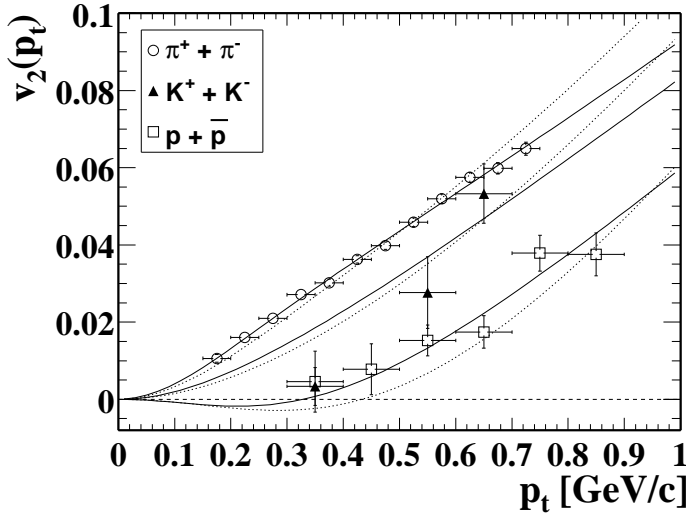


Fig. 10. Elliptic flow for pions, kaons and protons with fits from blast wave models [19].

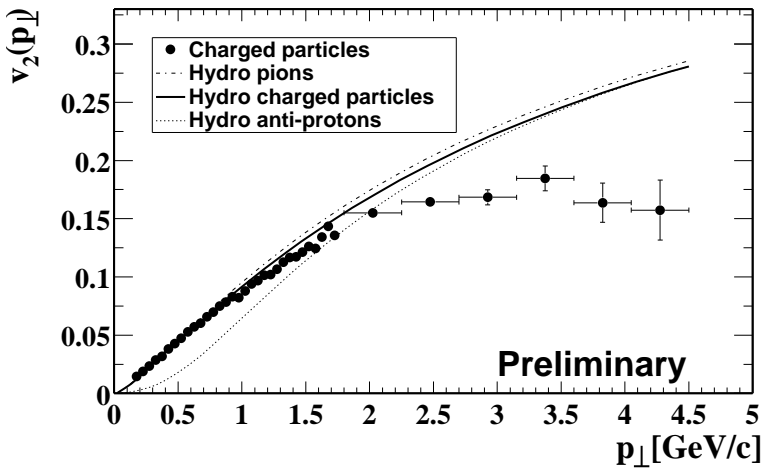


Fig. 11. Elliptic flow for charged particles at high p_T .

7. High p_T

Particles at high transverse momentum can be used to probe the fireball. High energy partons lose energy through a gluon radiation mechanism and predictions show that the magnitude of the energy loss (dE/dx) depends on the gluon density of the medium [20]. For this reason the suppression of hadrons may be an interesting QGP signature. The preliminary negative hadron distribution from the 5% most central data is shown in figure 12. Also shown for comparison are the negative hadron distributions for Pb+Pb collisions at $\sqrt{s_{NN}} = 170$ GeV and the charge averaged hadrons ($h^+ + h^-$)/2 from $p + \bar{p}$ collisions at $\sqrt{s_{NN}} = 200$ GeV. The STAR data appear to be flatter than the lower energy nuclear data points and the mean p_T is somewhat higher. A more detailed comparison to the elementary collision data is shown in figure 13 where the STAR data have been divided by the UA1 data using an appropriate scaling to account for the different energies and the nuclear overlap. At low p_T the yield initially scales with the number of

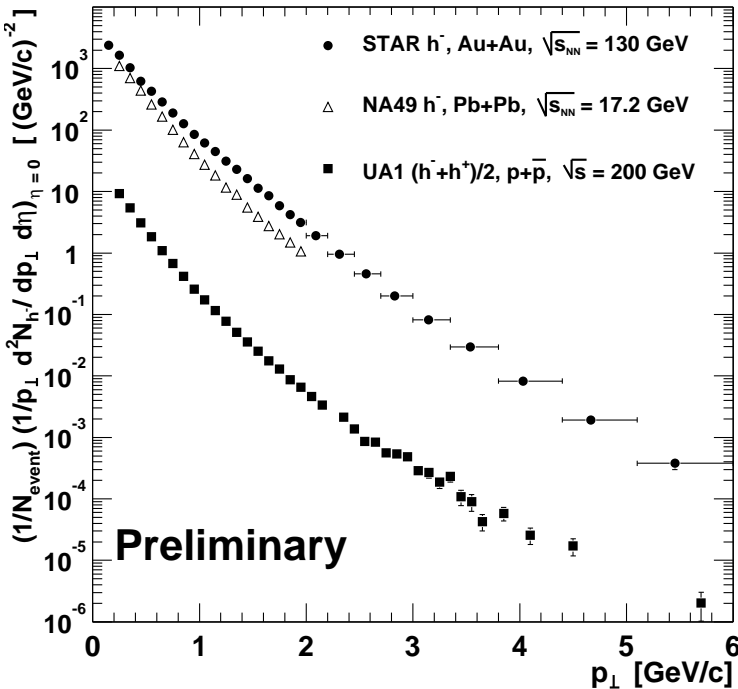


Fig. 12. Negative charged particle spectra compared with those obtained in $p + \bar{p}$ at $\sqrt{s_{NN}} = 200$ GeV and Pb+Pb at $\sqrt{s_{NN}} = 17$ GeV collisions by UA1 and NA49 collaborations, respectively.

binary collisions as expected. The data approach the binary collision scaling limit but at higher p_T start to decrease. This turn over could be interpreted as evidence for such an energy loss mechanism due to a larger dE/dx of partons in the hot QCD medium.

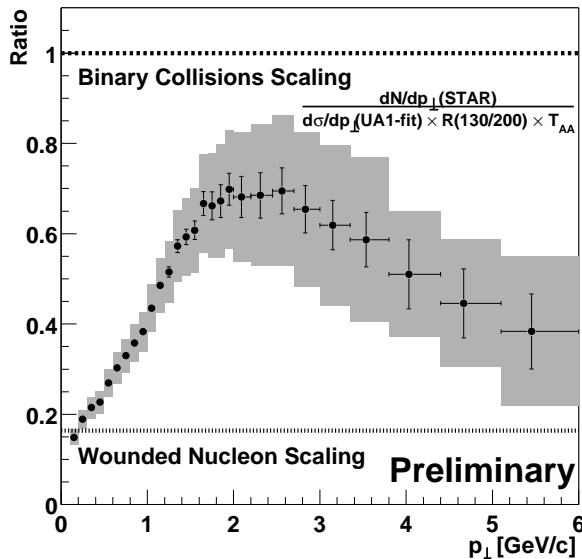


Fig. 13. Preliminary charged particle spectrum scaled to UA1 data. Error bars indicate the error on the measurement and the shaded parts are the total uncertainty including scaling factors.

8. Summary and future

The measurements of hadron production indicate that particles are produced from a source consistent with a chemical freeze-out temperature of approximately 170 MeV and with a high degree of radial flow. The high degree of elliptic flow as well as the very similar particle and anti-particle distributions indicate that particles undergo a large amount of re-scattering.

In the second year of RHIC running at $\sqrt{s_{NN}} = 200$ GeV three million event samples of both centrally-triggered and minimum bias events were recorded. Coupled with the addition of ZDC timing information, which provided more events in the centre of the TPC, this has resulted in an order of magnitude increase in the number of events available for physics analyses. This will enable STAR to produce spectra extending to higher p_T and to measure the elliptic flow for more particle species and thus examine the mass-dependence. We will also make more detailed analyses on centrality dependence and analyze the $p + p$ reference data which was also recorded.

REFERENCES

- [1] For reviews and recent developments see *Quark Matter 2001*, *Nucl. Phys.* **A698** (2002).
- [2] J. Letessier, A. Tounsi, J. Rafelski, *Phys. Lett.* **B292**, 417 (1992).
- [3] E. Andersen *et al.* [WA97 Collaboration], *J. Phys. G* **25**, 171 (1999).
- [4] M. Kaneta *et al.* [NA44 Collaboration], *J. Phys. G* **23**, 1865 (1997).
- [5] X.N. Wang, *Phys. Rev.* **C58**, 2321 (1998).
- [6] C. Adler *et al.* [STAR Collaboration], *Phys. Rev. Lett.* **87**, 112303 (2001).
- [7] G.J. Alner *et al.* [UA5 Collaboration], *Z. Phys.* **C33**, 1 (1986).
- [8] H. Appelshauser *et al.* [NA49 Collaboration], *Phys. Rev. Lett.* **82**, 2471 (1999).
- [9] B.B. Back *et al.* [PHOBOS Collaboration], *Phys. Rev. Lett.* **85**, 3100 (2000).
- [10] K. Adcox *et al.* [PHENIX Collaboration], *Phys. Rev. Lett.* **86**, 3500 (2001).
- [11] C. Adler *et al.* [STAR Collaboration], nucl-ex/0203016.
- [12] C. Adler *et al.* [STAR Collaboration], *Phys. Rev. Lett.* **87**, 262302 (2001).
- [13] N. Xu *et al.* [NA44 Collaboration], *Nucl. Phys.* **A610**, 175C (1996).
- [14] I.G. Bearden *et al.* [NA44 Collaboration], *Phys. Rev. Lett.* **78**, 2080 (1997).
- [15] J. Bachler *et al.* [NA49 Collaboration], *Nucl. Phys.* **A661**, 45 (1999).
- [16] E. Schnedermann, J. Sollfrank, U.W. Heinz, *Phys. Rev.* **C48**, 2462 (1993).
- [17] W. Florkowski, W. Broniowski, nucl-th/0203058.
- [18] P. Braun-Munzinger, D. Magestro, K. Redlich, J. Stachel, *Phys. Lett.* **B518**, 41 (2001).
- [19] C. Adler *et al.* [STAR Collaboration], *Phys. Rev. Lett.* **87**, 182301 (2001).
- [20] R. Baier, D. Schiff, B.G. Zakharov, *Ann. Rev. Nucl. Part. Sci.* **50**, 37 (2000).